Available online at www.sciencedirect.com
SCIENCE DIRECT
Polymer 46 (2005) 5986–5991
polymer
www.elsevier.com/locate/polymer

Effect of blending sequence on microstructure of ternary nanocomposites

Aravind Dasari, Zhong-Zhen Yu*, Yiu-Wing Mai

Center for Advanced Materials Technology (CAMT), School of Aerospace, Mechanical and Mechatronic Engineering J07, The University of Sydney, Sydney, NSW 2006, Australia

Received 4 December 2004; received in revised form 13 April 2005; accepted 19 May 2005
Available online 21 June 2005

Abstract

Knowledge of the nature of molecular processes occurring during melt compounding of nanomaterials and polymers is crucial in determining the ultimate performance of polymer nanocomposites. In this paper, we demonstrate for the first time with detailed transmission electron microscopy, the parameters that affect the microstructure of polymer nanocomposites by varying the blending sequence. Nylon 66/organoclay/SEBS-*g*-MA ternary nanocomposites prepared by four different blending sequences exhibited distinct microstructure and mechanical properties. It was concluded that the best microstructure for toughness and other mechanical properties is to have the maximum percentage of the exfoliated organoclay in the nylon 66 matrix rather than to have it in the dispersed SEBS-*g*-MA phase. The presence of organoclay in the SEBS-*g*-MA phase reduces the latter's ability to cavitate, resulting in reduced toughening efficiency.

Keywords: Microstructure; Nanocomposites; Blending sequence

1. Introduction

Polymeric materials can exhibit significantly improved mechanical properties if they possess multi-component phase separated morphology at the nanoscale [1]. The nano-domains can constrain the polymer chains or enhance the toughening efficiency of the polymer depending on the type of filler used. However, the extent of improvement is determined by the microstructure represented by the size, shape, and homogeneity of the reinforcement in the polymeric matrix [2]. Recent advances in the formulation and evaluation of the energetics and interatomic interactions in materials combined with the development and implementation of computational methods and simulation techniques led to the investigations of the microscopic origins of complex nano-domains in materials [3–5]. As the trend towards miniaturization of technological devices continues, nanoscale characterization of the morphology plays a dominant role.

Of the many types of nano-reinforcements available for polymers, clay has attracted the greatest interest in recent years, both in industry and in academia, because of the ability of the silicate particles to disperse into individual layers and the ability to fine tune their surface chemistry through ion exchange reactions with organic and inorganic cations. However, almost two decades after the introduction of the concept of polymer silicate nanocomposites, still substantial understanding of the parameters that result in a good balance between elastic stiffness and fracture toughness of these materials is needed. Many approaches have been adopted in the expectation of achieving this goal, such as by addition of an elastomeric phase to the polymer clay nanocomposites [6,7], usage of organoclay as a compatibilizer for immiscible polymer blends [8], and further modification of organically treated clay with epoxy monomer before blending to produce an intercalated nanocomposite [9]. These methods have resulted in improved tensile strength and elastic modulus along with a slight increase in toughness. The improvement was attributed to the enhanced dispersion quality and interfacial interaction between the dispersed phases in the matrix. Also, some mathematical models have been proposed to understand the reinforcement aspects of these nanocomoposites [10,11]. Despite all these, an in-depth understanding of the parameters affecting the mechanical properties of nano-composites, in particular, toughness is still lacking.

In this study, we used styrene-ethylene/butylene-styrene

* Corresponding author. Tel.: +61 2 935 17150; fax: +61 2 935 13760.
E-mail address: zhongzhen.yu@aeromech.usyd.edu.au (Z.-Z. Yu).

0032-3861/$ - see front matter © 2005 Elsevier Ltd. All rights reserved.
doi:10.1016/j.polymer.2005.05.145

triblock copolymer grafted with 1.84 wt% of maleic anhydride (SEBS-*g*-MA) as a toughening agent and a high polar organoclay as a reinforcing agent to obtain balanced toughness and elastic stiffness of nylon 66. SEBS-*g*-MA was selected as it was well established in the literature that during melt processing, the maleic anhydride grafted to SEBS reacts with the amine end groups on the nylon chain to form an in situ grafted copolymer, nylon 66-*co*-SEBS-*g*-MA, which allows SEBS-*g*-MA to be finely dispersed in the nylon matrix and simultaneously strengthens the interface between the phases [12]. This further helps to stabilize the obtained morphology. The objective of the present work is to provide an insight, with detailed transmission electron microscopy, on the parameters that affect the microstructure of polymer nanocomposites by varying the blending sequence.

2. Experimental work

2.1. Preparation of materials

Nylon 66, a polyamide resin with a trade name of Vydyne® 21PC, was supplied by Monsanto. Southern Clay Products Inc. supplied the organoclay having a cation exchange capacity of 90 mequiv/100 g (trade name of Cloisite® 30B) via Jim Chambers and Associates, Australia. The alkyl ammonium surfactant used in organoclay is methyl, tallow, bis-2-hydroxyethyl quaternary ammonium chloride. The loss on ignition of the organoclay is about 30 wt%. Styrene-ethylene/butylene-styrene triblock copolymer grafted with 1.84 wt% of maleic anhydride (SEBS-*g*-MA) was supplied by Shell Chemical Company under the trade name of Kraton FG 1901X. It has been reported that the ratio of styrene to ethylene/butylene in the triblock copolymer was 28/72 by wt% and the glass transition temperature of the SEBS-*g*-MA is −42 °C.

Prior to blending, nylon 66 and organoclay were dried at 90 °C under vacuum for 12 h. Nylon 66 composites were prepared in a Werner and Pfleiderer ZSK-30 twin-screw extruder ($L/D=30$, $L=0.88$ m) at a temperature of 260–280 °C and a screw speed of 300 rpm. To investigate the effect of blending nylon 66, organoclay, and SEBS-*g*-MA on the final microstructure, dispersion, and size of reinforcements, four blending sequences were adopted. (a) N1-(Nylon 66 + SEBS-*g*-MA + organoclay) (80/15/5) means nylon 66, SEBS-*g*-MA and organoclay were blended simultaneously; (b) N2-(Nylon 66 + SEBS-*g*-MA) + organoclay (80/15/5) means nylon 66 was blended with SEBS-*g*-MA first and the nylon 66/SEBS-*g*-MA blend was mixed with organoclay later; (c) N3-(Nylon 66 + organoclay) + SEBS-*g*-MA (80/5/15) means nylon 66 was reinforced with organoclay first and the nylon 66/organoclay nanocomposite was blended with SEBS-*g*-MA later; and (d) N4-Nylon 66 + (SEBS-*g*-MA + organoclay) (80/15/5) means SEBS-*g*-MA was mixed with organoclay and then the SEBS-*g*-MA/organoclay mixture was blended with nylon 66 later.

2.2. Mechanical testing

The notched impact strength (J/m) was evaluated in an ITR-2000 instrumented impact tester according to ASTM D256 on the injection molded rectangular bars machined with a 45° V-notch (depth of 2.54 mm). Flexural properties were determined in three-point bending mode in an Instron 5567 testing machine according to ASTM standard D790. The span distance and crosshead speed used were 100 mm and 2 mm/min, respectively. All these tests were conducted at ambient temperature (20–25 °C) and an average value of five repeated tests was taken for each composition.

2.3. Morphology observations and quantification

To investigate the dispersion of organoclay layers and SEBS-*g*-MA particles in nylon 66, ultra-thin sections ranging from 60 to 90 nm in thickness are cryogenically cut with a diamond knife in liquid nitrogen environment at −80 °C using a Leica Ultracut S microtome. Sections were collected on holey carbon grids and were carefully stained with osmium tetroxide (OsO_4) vapor to enhance the phase contrast among nylon 66, organoclay, and SEBS-*g*-MA. Subsequently, the thin sections were observed using a Philips CM12 transmission electron microscope at an accelerating voltage of 120 kV. Also, freeze-fractured experiments were conducted to study the dispersion and to estimate the particle size of the dispersed SEBS-*g*-MA in the nylon 66 matrix. Freeze-fractured surfaces were etched with xylene at ambient temperature for 12 h to remove the dispersed phase and then observed with a Philips S-505 scanning electron microscope (SEM). Then, the morphology of nanocomposites was quantified by image analysis to determine the dispersion of SEBS-*g*-MA in the nylon 66 matrix and the effect of clay layers on the dispersed SEBS-*g*-MA size distribution in ternary nanocomposites. A minimum number of 400 SEBS-*g*-MA particles were considered on each fractograph to identify the size distribution. The image analysis program used was Image J (based on an NIH software). Additionally, ultra-thin sections from the stress-whitened zones on the impact-fractured specimens were also prepared to study their nanoscale deformation behavior.

3. Results and discussion

X-ray diffraction patterns of the four ternary nanocomposites did not show any characteristic basal diffraction peak of organoclay in the range of $2\theta=1$–$10°$, irrespective of the blending sequence (not presented here), suggesting that the organoclay is fully exfoliated in all the ternary nanocomposites in the presence of SEBS-*g*-MA. However,

in contrast to this suggestion, distinct differences in the notched impact strength (Table 1) were observed. So, to better understand these seemingly inconsistent results, microstructural characterization of the ternary nanocomposites was carried out in detail with the aid of transmission electron microscopy. SEBS-*g*-MA particles were selectively stained with osmium tetroxide vapor to enhance the phase contrast amongst the three phases, nylon 66, SEBS-*g*-MA, and organoclay.

TEM micrographs of N1–N4 in Fig. 1 clearly show distinctly different dispersions of the organoclay and SEBS-*g*-MA phases in nylon 66 matrix and the final microstructure. In N1 and N2, it can be seen that the SEBS-*g*-MA particles are finely dispersed in the nylon 66 matrix. This suggests that the in situ formed nylon 66-*co*-SEBS-*g*-MA copolymer (when nylon 66 and SEBS-*g*-MA were blended prior to mixing with clay or when all three components were blended simultaneously) helps in finely dispersing the SEBS-*g*-MA phase, hence improving the interfacial interaction. However, depending on the interaction of organoclay with nylon 66 matrix and SEBS-*g*-MA particles, both exfoliated and intercalated structures are evident from each of the TEM micrographs (Fig. 1: N1 and N2). As nylon 66 has a higher polarity than SEBS-*g*-MA, silicate layers of organoclay are easily exfoliated in the nylon 66 matrix, whereas thick platelets of organoclay are evident in the SEBS-*g*-MA phase, suggesting an intercalated structure. It is also speculated that the shear force produced during twin-screw extrusion of the samples may be insufficient for the organoclay present in the cross-linked SEBS-*g*-MA phase to delaminate and allow more SEBS-*g*-MA into its intra-galleries to produce an exfoliated structure. Additionally, the percentage of organoclay seems to be equally distributed between nylon 66 matrix and SEBS-*g*-MA phase in N1 and N2. Even though similar microstructure is present in N1 and N2, the observed differences in the notched impact strength can be attributed to the blending sequence. In comparison to N1, in N2, SEBS-*g*-MA was extruded twice (initially with nylon 66, and then the blend with organoclay), giving the SEBS-*g*-MA phase ample time in the twin-screw extruder to enhance its cross-linking ability. The cross-linking restricts the elasticity of SEBS-*g*-MA by increasing the rigidity of the phase, thereby, ultimately decreasing its toughening efficiency. Another parameter, which is also believed to influence the toughening efficiency, is the SEBS-*g*-MA particle size. However, considering the small differences in particle sizes of N1 and N2 (see below for mean average size of SEBS-*g*-MA in N1 and N2), it can be concluded that this parameter plays a less dominant role in the present study.

N3 (with the highest impact strength), prepared by initially blending nylon 66 and organoclay and afterwards with SEBS-*g*-MA, although shows an increase in the particle size of SEBS-*g*-MA, an important aspect of this blending sequence is that most of the organoclay is present in the nylon 66 matrix (Fig. 1). This is in contrast to N1 and N2, where similar percentage distribution of organoclay was observed in both the nylon 66 and SEBS-*g*-MA phases. The organoclay in N3 exhibited a truly exfoliated structure in the nylon 66 matrix (see also Fig. 2 for a high magnification TEM micrograph of N3). It is also interesting to note that some amount of the organoclay in N3 is present at the interface of nylon 66 and SEBS-*g*-MA, encapsulating the SEBS-*g*-MA particles from the nylon 66 matrix. The reason for this type of morphology may be explained as follows: in N3, the nylon 66/organoclay nanocomposite is first prepared in which the polar organoclay is exfoliated due to its affinity with the amine end groups on nylon 66 and a strong interaction exists between them. Now, if SEBS-*g*-MA is added, the exfoliated organoclay may be attracted towards the SEBS-*g*-MA phase due to the presence of the maleic anhydride groups. However, the already present strong interaction of exfoliated organoclay in the nylon 66 matrix prevents the organoclay from entering the cross-linked SEBS-*g*-MA phase, finally resulting in an amount of the organoclay present at the interface between nylon 66 and SEBS-*g*-MA phases, which resembles a hard shell to the soft core SEBS-*g*-MA phase. Nevertheless, the important point to be noted here is that most of the organoclay in N3 is

Table 1
Mechanical properties along with their compositions of ternary nanocomposites (N1–N4) prepared by different blending sequences

Blending sequence	Notched impact strength (J/m)	Flexural modulus (GPa)	Flexural strength (MPa)
Neat nylon 66	62.5±3.3	2.95±0.05	129.0±3.8
Nylon 66/organoclay (80/5)	23.9±6.0	3.79±0.10	66.8±5.5
Nylon 66/SEBS-*g*-MA (80/15)	303.4±56.2	2.06±0.15	92.4±7.3
N1, (nylon 66+SEBS-*g*-MA+organoclay) (80/15/5)	102.9±10.6	2.54±0.11	98.5±2.5
N2, (nylon 66+SEBS-*g*-MA)+organoclay (80/15/5)	78.9±3.9	2.53±0.07	96.8±2.7
N3, (nylon 66+organoclay)+SEBS-*g*-MA (80/5/15)	117.6±16.3	2.65±0.03	100.7±0.2
N4, nylon 66+(SEBS-*g*-MA+organoclay) (80/15/5)	65.9±3.9	2.63±0.02	98.9±1.1

Additionally, the mechanical properties of neat nylon 66, nylon 66/organoclay binary nanocomposite, and nylon 66/SEBS-*g*-MA binary blend are also given to differentiate the effect of addition of stiff organoclay and soft SEBS-*g*-MA phase.

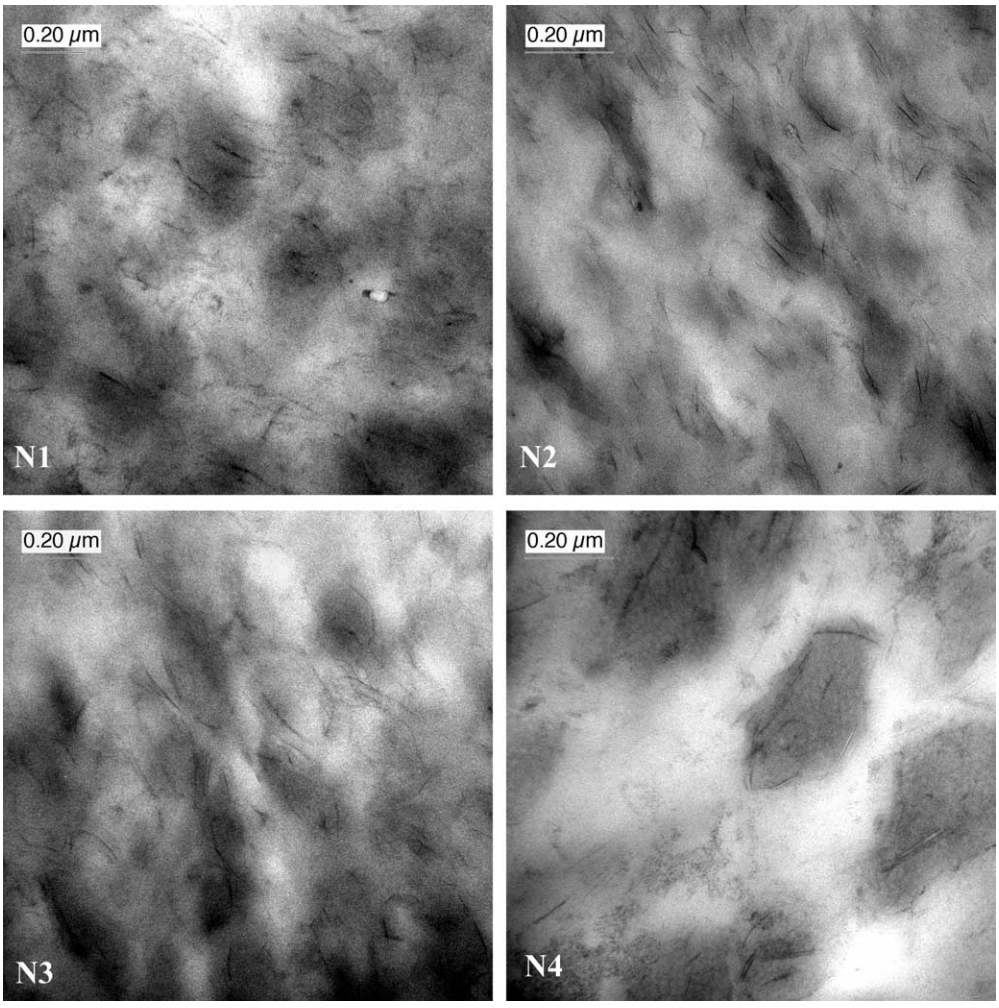

Fig. 1. TEM micrographs of nylon 66/organoclay/SEBS-*g*-MA ternary nanocomposites prepared by different blending sequences, N1, N2, N3, and N4.

present in the continuous nylon 66 matrix rather than in the soft domains of SEBS-*g*-MA phase.

On the contrary, N4, which has the lowest impact strength, exhibits a completely different behavior from N3 and N1 or N2. As organoclay is blended with SEBS-*g*-MA first, most of the organoclay is present in the SEBS-*g*-MA phase (Fig. 1: N4 and Fig. 2: N4). However, the relatively low polar nature of SEBS-*g*-MA cannot exfoliate the silicate

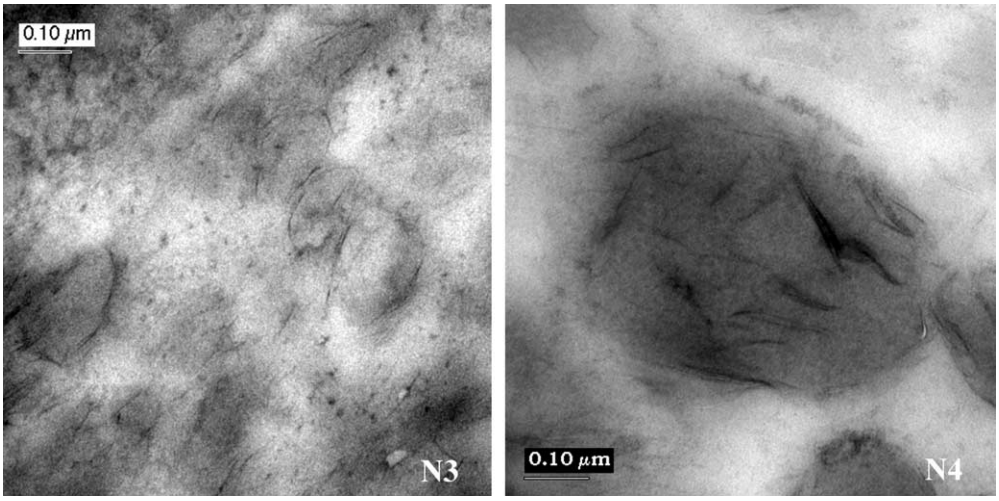

Fig. 2. High magnification TEM micrographs of N3 and N4 showing the distinct microstructure.

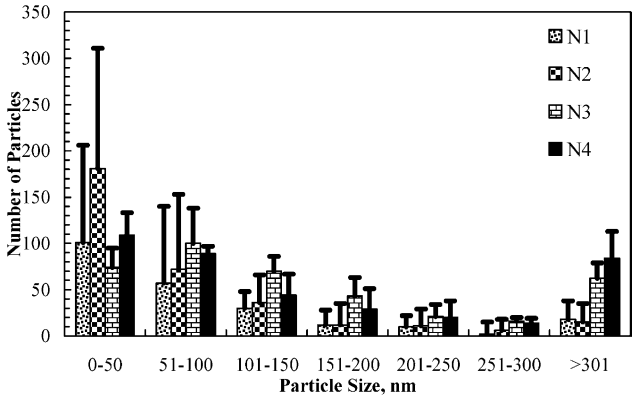

Fig. 3. Dispersed SEBS-*g*-MA particle size distribution in N1, N2, N3, and N4.

layers, and results in an intercalated structure in the SEBS-*g*-MA phase. Additionally, the SEBS-*g*-MA particle size is very large in N4 in comparison to N1, N2, and N3. This may be due to the fact that the interaction between the maleic anhydride groups of SEBS-*g*-MA and the hydroxyethyl groups of the organoclay suppresses the dispersion of SEBS-*g*-MA in the nylon 66 matrix. To further obtain a quantitative understanding of the dispersion of SEBS-*g*-MA phase, scanning electron micrographs of freeze-fractured ternary nanocomposites are analyzed by the image analysis program, 'Image J'. A minimum number of 400 SEBS-*g*-MA particles are considered on each fractograph to identify the size distribution (Fig. 3). The mean particle sizes of SEBS-*g*-MA particles in N1, N2, N3, and N4 are 120, 137, 202, and 281 nm, respectively, which are consistent with the TEM micrographs.

The TEM observations described above are apparently contradictory to the results of XRD and can be ascribed to the location of organoclay in the ternary nanocomposites. In N1–N3, organoclay in the fully exfoliated structure is located in the nylon 66 matrix and is believed to be responsible for the absence of diffraction peak of organoclay between 1 and 10° in the XRD patterns. The intercalated organoclay embedded in the finely dispersed SEBS-*g*-MA phase in the nylon 66 matrix is not detected in the XRD. Additionally, in N4, the absence of the diffraction peak of organoclay is due to the minimum amount or absence of organoclay in the nylon 66 matrix rather than clay exfoliation. In fact, most of the organoclay is in the dispersed SEBS-*g*-MA phase with an intercalated structure.

From the above discussions of the different blending sequences, it is evident that the different impact strength results are largely caused by the location of the organoclay in the nanocomposites. It seems beneficial in terms of impact strength (toughness) to have a maximum percentage of the exfoliated organoclay in the nylon 66 matrix. Conversely, it is detrimental to have organoclay in the SEBS-*g*-MA phase, irrespective of an exfoliated or intercalated structure. This is because the organoclay stiffens the SEBS-*g*-MA phase and reduces the latter's ability to cavitate so that the toughening efficiency of the SEBS-*g*-MA is decreased. An illustration of this is presented in Fig. 4. TEM micrographs of the stress-whitened zone on the impact fractured specimens in N3 and N4 clearly delineate the differences in the ability of SEBS-*g*-MA to cavitate. The reduced intensity of cavitation of SEBS-*g*-MA phase in N4 is detrimental to the toughening efficiency of SEBS-*g*-MA. Additionally, considering the notched impact strength differences between N1 and N3 (only ~15–20% higher in N3), it seems reasonable to say that a two-step compounding process does not have a significant influence on the mechanical properties compared to a single-step compounding. However, it should be noted that N3 has a mean SEBS-*g*-MA particle size of 202 nm as compared to N1 of 120 nm. It is expected that by reducing the SEBS-*g*-MA particle size in N3 to that of N1 or even finer, significant improvement in impact strength (toughness) can be achieved along with other mechanical

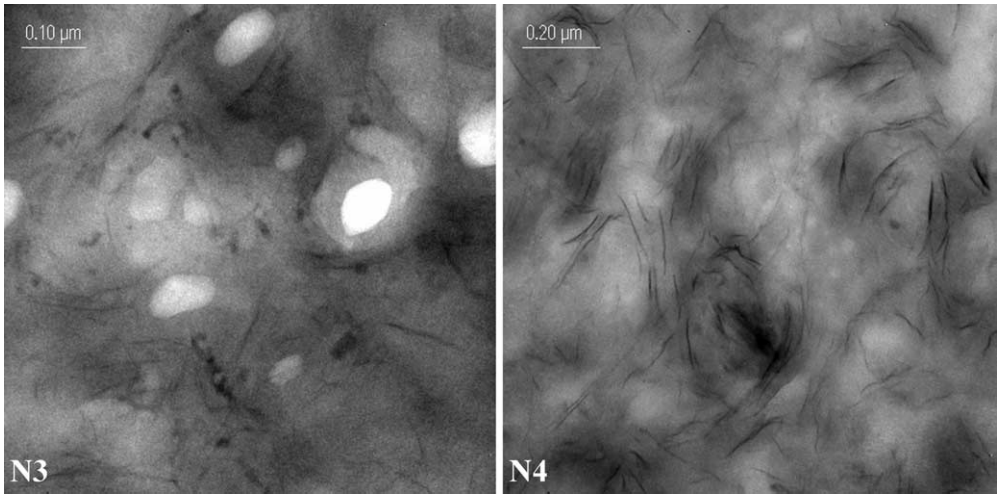

Fig. 4. TEM micrographs of stress-whitened zone in N3 and N4 delineating the differences in the ability of SEBS-*g*-MA to cavitate (cavities are shown as bright white areas in N3).

properties. Thus, the best microstructure for impact strength and other mechanical properties is to have a maximum percentage of the exfoliated organoclay in the nylon 66 matrix rather than to have it in the SEBS-*g*-MA phase.

4. Conclusions

The microstructure in ternary nanocomposites was significantly influenced by the blending sequence, which influenced their mechanical properties, particularly, notched impact strength. It was shown that blending nylon 66 and organoclay initially and later mixing with SEBS-*g*-MA is the preferred blending sequence to maximize the notched impact strength. The differences in impact strength are largely caused by the location of the organoclay in the nanocomposites. It is beneficial in terms of impact strength to have the maximum amount of the exfoliated organoclay in the nylon 66 matrix. In contrast, it is detrimental to have organoclay in the SEBS-*g*-MA phase, irrespective of an exfoliated or intercalated structure as the presence of organoclay reduces the cavitation ability of SEBS-*g*-MA particles.

Acknowledgements

The authors thank the Australian Research Council (ARC) for the continuing support of this project on: 'Polymer Nanocomposites'. Y.W.M. and Z.-Z.Y. are, respectively, Australian Federation Fellow and Australian Postdoctoral Fellow, supported by the ARC and tenable at the CAMT, University of Sydney. A.D. thanks the Australian Government for an International Postgraduate Research Scholarship award and the University of Sydney for an International Postgraduate award to undertake a PhD program in the CAMT.

References

[1] Kietzke T, Neher D, Landfester K, Montenegro R, Guntner R, Scherf U. Nat Mater 2003;2:408.
[2] Kojima Y, Usuki A, Kawasumi M, Okada A, Fukushima Y, Kurauchi T, et al. J Mater Res 1993;8:1185.
[3] Bhushan B, Israelachvili JN, Landman U. Nature 1995;374:607.
[4] Aoike T, Uehara H, Yamanobe T, Komoto T. Langmuir 2001;17: 2153.
[5] Bhushan B. Handbook of micro/nanotribology. 2nd ed. Boca Roton, FL: CRC Press; 1999.
[6] Khatua BB, Lee DJ, Kim HY, Kim JK. Macromolecules 2004;37: 2454.
[7] Li X, Park HM, Lee JO, Ha CS. Polym Eng Sci 2002;42:2156.
[8] Wang Y, Zhang Q, Fu Q. Macromol Rapid Commun 2003;24:231.
[9] Liu XH, Wu QJ. Macromol Mater Eng 2002;287:180.
[10] Fornes TD, Paul DR. Polymer 2003;44:4993.
[11] Sheng N, Boyce MC, Parks DM, Rutledge GC, Abes JI, Cohen RE. Polymer 2004;45:487.
[12] Kayano Y, Keskkula H, Paul DR. Polymer 1997;38:1885.